10-2015

Characterize Behavior of Geogrid Reinforced Ballast at Different Levels of Degradation Through Triaxial Shear Strength Test and Discrete Element Modeling

Yu Qian
University of Illinois, Urbana-Champaign

Debakanta Mishra
Boise State University

Erol Tutumluer
University of Illinois, Urbana-Champaign

Hasan A. Kazmee
University of Illinois, Urbana-Champaign

Characterize Behavior of Geogrid Reinforced Ballast at Different Levels of

Degradation through Triaxial Shear Strength Test and Discrete Element

Modeling

Yu Qian[1], Debakanta Mishra[2], Erol Tutumluer[3], and Hasan A. Kazmee[4]

[1]Ph.D., Research Engineer, Department of Civil and Environmental Engineering, the University of Illinois at Urbana-Champaign, Urbana, Illinois 61801, USA; tel: 1-2177994558; fax: 1-2173339464; email: yuqian1@illinois.edu (*Corresponding author*)

[2]Ph.D., Assistant Professor, Department of Civil Engineering, Boise State University, Boise, Idaho 83725, USA; formerly Post-Doctoral Research Associate at the University of Illinois at Urbana-Champaign; tel: 1-2084262351; fax: 1-2084262351; email: debmishra@boisestate.edu

[3]Ph.D., Professor, Department of Civil and Environmental Engineering, the University of Illinois at Urbana-Champaign, Urbana, Illinois 61801, USA; tel: 1-2173338637; fax: 1-2173331924; email: tutumlue@illinois.edu

[4]Ph.D. Student, Graduate Research Assistant, Department of Civil and Environmental Engineering, the University of Illinois at Urbana-Champaign, Urbana, Illinois 61801, USA; tel: 1-2174199971; email: kazmee2@illinois.edu

ABSTRACT

Recent research efforts at the University of Illinois have aimed at studying geogrid applications in railroad track structures, specifically focusing on ballast and subballast reinforcement. Ballast, typically comprising large sized aggregate particles with uniform gradation, is an essential layer in the railroad track substructure to facilitate load distribution and drainage. The primary mechanism of load transfer within the ballast layer involves inter-particle contact between ballast particles. Similarly, the effectiveness of ballast reinforcement with geogrids is primarily governed by the geogrid-aggregate interlock. Such interaction and the effectiveness thereof can change significantly as the level of grain size and shape degradation or

fouling increases in the ballast layer with accumulation of train traffic. Although several studies in the past have investigated the effects of geogrid reinforcement on ballast shear strength and permanent deformation behavior, the effectiveness of geogrid reinforcement at different levels of ballast degradation needs to be further understood. In this study, monotonic triaxial shear strength tests were conducted on both new and degraded ballast materials with and without geogrid reinforcement. Two geogrid types, with square- and triangular-shaped apertures, were used in the laboratory to calibrate an aggregate imaging-based Discrete Element Method (DEM) modeling approach, which is capable of creating actual ballast aggregate particles as three-dimensional polyhedron blocks having the same particle size distributions and imaging quantified average shapes and angularities. The DEM model was observed to adequately capture the shear strength behavior of geogrid-reinforced triaxial ballast specimens prepared using both new and degraded ballast samples.

Keywords: geosynthetics, railroad ballast, geogrid, triaxial testing, discrete element method, ballast fouling, degradation

INTRODUCTION

Geogrids have been successfully used in railroad applications to construct railroad track over weak subgrades as well as reinforce ballast layer for improved lateral stability and reduced track settlement. For subgrade stabilization, the geogrids

are often placed at the bottom of subballast and on top of the subgrade. Ballast reinforcement benefit of using geogrids is realized by limiting the lateral movement of aggregate particles. For this purpose, the geogrids are commonly installed at the ballast-subballast interface. The degree of interlocking to be maximized between geogrids and ballast particles is governed by several factors acting in combination, e.g., aggregate size and shape properties, geogrid types and properties (such as apertures, shapes and sizes of ribs, etc.), compactive effort during installation, and loading conditions.

The benefits of geogrid reinforcement have been highlighted by several laboratory research efforts, numerical simulations, as well as field implementation programs (Bathurst and Raymond 1987, Raymond and Ismail 2003, Indraratna et al. 2006, McDowell et al. 2006, Brown et al. 2007, Tutumluer et al. 2009, Qian et al. 2011, Chen et al 2012, Qian et al. 2013a-b, Mishra et al. 2014). These previous research studies have also identified subgrade conditions, number of geogrid layers, geogrid installation depth, presence of moisture, aggregate size to geogrid aperture size ratio, geogrid aperture shape, etc. to be important controlling factors as far as geogrid reinforcement of railroad ballast is concerned. However, most of the current findings reported in the literature primarily focus on the performances of relatively new track sections where clean ballast with not much degradation was used in the beginning of its service life.

With the accumulation of tonnage in the field, ballast layers are progressively "fouled" with finer materials filling the void space within the coarse particle matrix. Although subgrade intrusion as well as spillage of foreign materials such as coal dust can contribute to the fouling phenomenon, degradation of ballast particles has been reported to contribute up to 76% of the total ballast layer fouling (Selig and Waters, 1994). The gradual filling up of voids in a ballast matrix due to particle degradation has been schematically represented in Fig. 1. Note that gradual degradation of ballast particles leads to considerable changes in the aggregate size and shape properties as well as ballast packing. Moreover, increasing degrees of fouling has the potential to significantly affect geogrid-aggregate interlock mechanisms. Such effects of ballast degradation on ballast strength and aggregate-geogrid interlock have not been thoroughly studied.

This paper describes preliminary findings from an ongoing research study at the University of Illinois focusing on triaxial testing of geogrid-reinforced ballast specimens using a large-scale triaxial test device and modeling the micromechanical interactions of geogrid-aggregate systems using the Discrete Element Method (DEM). Cylindrical triaxial specimens were prepared using new as well as degraded ballast materials reinforced with geogrids having either triangular or square shaped apertures. Monotonic triaxial shear strength tests were conducted to evaluate the reinforcement benefits through improved stress-strain behavior and shear strength properties. Unreinforced ballast specimens were also tested to serve as the control sets during this

study. To simulate the triaxial tests and investigate geogrid reinforcement mechanisms, a numerical modeling approach based on the DEM was adopted with the capability to create actual ballast aggregate particles as three-dimensional polyhedron elements having the same particle size distributions and imaging quantified average shapes and angularities. Both the laboratory triaxial strength tests and the DEM simulation results are presented in this paper to evaluate the reinforcement benefits and mechanisms governing behavior of the ballast specimens reinforced with different geogrid types.

TRIAXIAL TEST DEVICE

A large-scale triaxial test device (The University of Illinois Ballast Triaxial Tester or TX-24) was recently developed at the University of Illinois for testing ballast size aggregate materials (Mishra et al. 2013). The test specimen dimensions are 305 mm (12 in.) in diameter and 610 mm (24 in.) in height. An internal load cell (Honeywell Model 3174) with a capacity of 89 kN (20 kips) placed on top of the specimen top platen measures accurately the applied load levels. Three vertical Linear Variable Differential Transformers (LVDTs) are mounted on the cylindrical test specimen at 120-degree angles to measure the vertical deformations of the specimen from three different side locations. Another LVDT is mounted on a circumferential chain wrapped around the specimen at the mid-height to measure the radial deformation of the test specimen. Fig. 2 shows a photograph of the TX-24 setup having an instrumented ballast specimen ready for shear strength testing.

To adequately simulate the high loading rates associated with train movements, ballast specimens in this study were tested for shear strength properties by imposing a rapidly applied axial strain at a rate of 5% per second under a constant all-around confining pressure level of 138 kPa (20 psi) (Qian et al. 2013c). Considering the 610-mm (24-in.) high ballast specimens, such a loading rate corresponds to vertical ram movements of 30.5 mm (1.2 in.) per second. As such large movements of the loading ram are likely to cause instant bulging and shearing of the ballast specimens, the LVDTs were not mounted directly on the specimen during the shear strength testing. Accordingly, axial deformations of the specimens were recorded directly from the internal LVDT within the hydraulic actuator.

BALLAST MATERIALS AND GEOGRIDS

The ballast material used in this study comprised 100% crushed limestone aggregates, and was tested under oven-dried conditions. Degradation of ballast under train loading was simulated through Los Angeles (LA) abrasion testing of the new limestone ballast. A 10-kg representative sample (in terms of gradation and shape properties) of oven-dried clean new ballast was subjected to LA abrasion testing for 1,500 turns to generate the material representing "fully fouled" conditions. Note that the extent of degradation achieved after 1,500 LA abrasion cycle corresponded to a Fouling Index (FI, defined as the sum of percent by weight of material passing the 4.75 mm and 0.075 mm sieve sizes) of 40. Such a value of FI has been established to correspond to a heavily fouled or degraded ballast condition requiring immediate

1   track maintenance activities (Selig and Waters 1994). The degraded ballast materials

2   thus generated were collected for conducting the triaxial shear strength tests and

3   labelled as "Degraded Materials with Fines." Subsequently, all particles finer than 9.5

4   mm (3/8 in.) were removed from the degraded materials, and the resulting material

5   (with all particles coarser than 9.5 mm or 3/8 in.) was labelled as "Degraded Ballast

6   without Fines." In the context of this paper, the term "Fines" refers to all particles

7   finer than 9.5 mm or passing the 3/8-in. sieve size. Such laboratory degradation effort

8   of the ballast material inside the LA abrasion drum was repeated until sufficient

9   amount of degraded ballast material was generated to prepare the triaxial test

10   specimens. More details on the steps followed to obtain the degraded ballast through

11   the LA abrasion testing have been provided elsewhere (Qian et al. 2014). Fig. 3 shows

12   the grain size distributions of the new ballast material confirming to the US AREMA

13   (American Railway Engineering and Maintenance of Way Association) No. 24

14   gradation requirements, along with the gradation curves for the degraded ballast

15   material with and without fines.

16

17   It is important to note that although the importance of ballast gradation in

18   governing the load carrying and drainage functionalities of ballast layers is widely

19   recognized establishing direct links between gradation information and mechanisms

20   governing ballast layer structural characteristics and drainage behavior is not trivial.

21   Accordingly, to investigate particle contact and particle packing characteristics before

22   and after degradation, approximately 10 kg each of the new and degraded (after 1,500

turns in the LA abrasion drum) ballast materials were placed in an acrylic chamber

with dimensions of 254 mm (10.0 in.) in diameter and 254 mm (10.0 in.) in height.

Fig. 4 shows photographs of the side and top views of the acrylic chamber filled with

ballast under the three conditions represented in Fig. 3. Photographs of the degraded

ballast without fines are also included in Fig. 4 for comparison purposes. It is clearly

seen that after 1,500 turns, the same weight (about 10 kg) of degraded ballast

occupied less volume compared to the new ballast in the acrylic chamber. However,

for the same weight of degraded ballast, the specimen height remained nearly the

same with or without fine particles as shown in Fig. 4. Accordingly, fines generated

during the degradation process occupied the voids created by the large particles

(particle sizes larger than 9.5 mm or 3/8 in.). At a degradation level corresponding to

$FI = 40$, nearly all the voids created by the large particles were filled with fines.

Beside the grain size distribution, imaging based aggregate shape properties,

i.e., the flat and elongated (F&E) ratio, the angularity index (AI), and the surface

texture (ST) index, are key indices affecting railroad ballast performance and can be

quantified by the University of Illinois Aggregate Image Analyzer (UIAIA) (Rao et al.

2002, Pan et al., 2006). The new and degraded ballast materials generated from the

LA abrasion test in this study were scanned using the recently enhanced UIAIA or

E-UIAIA, which utilizes three high resolution progressive scan type color cameras

and the improved color thresholding (E-UIAIA) technique. The imaging-based

morphological indices (F&E ratio, AI, and ST index) were then established to

generate ballast aggregate particle shapes as three-dimensional (3D) polyhedrons

utilized in the ballast DEM model (see Fig. 5). Note that particles finer than 9.5 mm

were not scanned using the E-UIAIA since these small sized particles were not

created as 3D polyhedron elements in the elements in the DEM simulations.

Accordingly, shape properties of different ballast materials discussed in this paper

correspond to the averaged values of particles larger than 9.5 mm (3/8 in). Table 1

lists a summary of the E-UIAIA determined imaging-based morphological indices and

certain gradation parameters of the ballast materials studied.

Each ballast sample studied (approximately 70 kg for new ballast, 73 kg for

degraded ballast without fines, and 94 kg for degraded ballast with fines) was poured

into an aluminum split mold in four lifts, and each lift was compacted using a 27.2-kg

(60-lb.) electric jack hammer for 4 seconds (16 seconds in total).   After compaction

of the first two lifts, one layer of geogrid was placed carefully in the middle of the test

specimen for making a geogrid reinforced ballast sample.   When compaction of all

four lifts was completed, each test specimen was checked for the total height and

leveling of the top plate. The specimen void ratios computed were 0.68 for new

ballast, 0.61 for degraded ballast without fines, and 0.25 for degraded ballast with

fines. Fig. 6 shows photographs of the geogrids used in the current study, and the

relevant properties of the geogrids are listed in Table 2.

DEM SIMULATIONS OF TRIAXIAL SHEAR STRENGTH TESTS

1   Several recent research studies have reported successful applications of the

2   Discrete Element Method (DEM) for simulating railroad ballast behavior (Indraratna

3   et al. 2010, Lu and McDowell 2010, Chen et al 2012, Tutumluer et al. 2013). The

4   DEM simulation approach developed at the University of Illinois (Ghaboussi et al

5   1990, Zhao et al. 2006, Nezami et al 2007) adopts real polyhedral particles and has

6   the capability to create actual ballast aggregate particle shapes as 3D polyhedron

7   elements having the same particle size distributions and imaging-quantified average

8   shapes and angularities. This DEM approach was calibrated by the laboratory large

9   scale direct shear test results (Tutumluer et al. 2006), validated by field track

10   settlement predictions (Tutumluer et al. 2013), and has been successfully utilized to

11   simulate complex ballast behavior, especially large scale triaxial tests with or without

12   geogrid reinforcement. (Qian et al. 2013a-b-c; Mishra et al. 2014).

13

14   Lee et al. (2012) used rigid rectangular cuboid discrete elements positioned in

15   a cylindrical arrangement to simulate a flexible membrane and followed an

16   "incremental displacement shearing method" to simulate triaxial shear strength tests

17   of sand using the BLOKS3D DEM program. Similarly, the BLOKS3D code has been

18   used by Qian et al. (2013c) to simulate large-scale triaxial shear strength tests of

19   ballast materials, as well as in this study to simulate large-scale triaxial shear strength

20   tests of degraded ballast materials with geogrid reinforcement. Fig. 7 provides an

21   overview of the BLOKS3D DEM model and corresponding modeling parameters are

22   listed in Table 3. Details of simulating a flexible membrane of the cylindrical test

1   specimen by rigid discrete elements and application of "incremental displacement

2   shearing method" in triaxial strength test simulation are provided elsewhere (Qian et

3   al. 2013c). With the "incremental displacement" shearing method, the CPU time

4   required to complete the triaxial shear strength simulations using a standard quad-core

5   PC was approximately 30 hours for the new ballast material, and slightly longer for

6   degraded ballast without fines. Note that for specimens prepared using the degraded

7   ballast material with fines, it was not possible to collect particle shape properties for

8   the fine particles for constituting the triaxial specimen within the DEM environment.

9   Moreover, the inclusion of numerous fine particles in the model would dramatically

10   increase the computational expense, with the estimated CPU time to complete one

11   simulation being in hundreds of days. Accordingly, the DEM simulations of triaxial

12   shear strength tests performed under the scope of the current study were only limited

13   to specimens prepared with new ballast and degraded ballast without fines.

14

15   After first establishing the membrane elements, approximately 500 particles,

16   having the same gradation and shape properties of the actual limestone ballast

17   material, were poured into the cylinder in two different sets. In between, a sheet of

18   geogrid element was generated corresponding to the different reinforcement

19   conditions being simulated. The geogrid element was modeled as a rigid

20   non-deformable element with the same aperture dimensions as the geogrids used in

21   experimental study. However, note that the rib thickness of the square aperture

22   geogrid could not be accurately modeled using the DEM approach. This was because

the rib thickness for the square aperture geogrid was significantly smaller than the individual ballast particle sizes. Modeling the exact rib dimensions of the square aperture geogrid would significantly increase the required computational effort. The rib thickness for the square aperture geogrid was therefore modeled in the current study as equal to that for the triangular aperture geogrid. Accordingly, the DEM simulated results for specimens with the square aperture geogrids are likely to overestimate the deviator stress values compared to the laboratory test results owing to the relatively thicker rib thicknesses.

LABORATORY TESTS AND DEM SIMULATION RESULTS

Fig. 8 presents results from large-scale triaxial shear strength tests conducted on the new and degraded limestone specimens for up to 10% axial strain. Peak deviator stress values for the different ballast materials obtained from laboratory experiments and DEM simulations are listed in Table 4. As shown in Fig. 8, all specimens exhibited similar stress-strain behavior under small magnitudes of imposed axial strains. This was primarily because under small imposed axial strain and corresponding small radial bulging conditions, the aggregate-geogrid interlock mechanism is not fully mobilized. However upon gradual increase in the axial strain levels, significant interlock between the geogrid and ballast particles is achieved to prevent lateral movements of particles and the corresponding radial bulging is prevented.

It is important to note that significant "jumps" in the stress-strain curve are observed at high axial strain levels. This can be attributed to the sudden breakage of geogrid ribs (often observed upon examining the geogrids after tests were completed in the laboratory), under excessive ballast-geogrid interaction forces or ballast particle breakage, and subsequent reorientation of individual ballast particles. As a certain geogrid rib or aggregate particle breaks, the adjacent ballast particles reorient themselves, and the system attains a new configuration with new interlocks formed between aggregate particles and the geogrid. This results in a restoration of the specimen shear strength until the next breakage of a geogrid rib occurs. The DEM simulation results presented in Fig.8 showed generally good agreement with the experimental data. In some cases, the DEM simulations overestimated the strength of geogrid reinforced specimens; this is due to the fact that breakage of the geogrid ribs or aggregate particles was not allowed in the DEM simulations.

Another interesting phenomenon observed from both the experimental and DEM simulation results is that particle degradation did not result in significant strength loss for the ballast specimens when compared with the new ballast material. On the contrary, in most cases the degraded ballast with or without fines yielded higher strength than new ballast. Comparing the gradations of the three ballast materials used in this study (see Fig. 3), the degraded ballast without fines comprised higher number of smaller particles, and was more "well" graded compared to the new ballast material satisfying AREMA No. 24 uniform gradation specification. The smaller particles within the degraded ballast matrix can potentially help stabilize the

aggregate skeleton, thus resulting in higher shear strength. Moreover, from the

imaging-based shape properties listed in Table 1, the degraded ballast particles have

significantly lower Angularity Index (AI), and tend to be more cubical and smoother

and hence less susceptible to abrading of sharp corners and edges during strength

testing when compared to the new ballast particles. Accordingly, more cubical

degraded ballast particles with smoother surfaces can attain a denser packing

configuration leading to higher densities for the specimens. This in turn results in

higher peak deviator stress values achieved during shear strength testing. Note that a

similar trend was reported by Tutumluer et al. (2013) when ballast with lower

angularity yielded less settlement in the field due to better packing.

For the specimens prepared with the degraded ballast material with fines, most

of fines (material finer than 9.5 mm or 3/8 in.) filled the void created by larger

particles (see Fig. 4), thus helping to stabilize the aggregate skeleton. However,

presence of excessive fines in the aggregate matrix results in the loss of contact

between large particles, thus making it easier for the large particles to reorient and

rearrange. This in-turn can lead to significant reductions in the specimen shear

strength. The fine particles thus present stabilization and also lubrication effects in the

specimens prepared with the degraded ballast material with fines. This was the reason

that degraded ballast with fines had lower strength than degraded ballast without fines

but higher strength than new ballast. This was also the reason that the degraded ballast

with fines had much smoother stress-strain curves during strength tests. However, all

1   the test results presented here were under dry conditions, which means no moisture

2   was involved in the test specimens. Upon introduction of moisture into the specimens,

3   the shear strength behavior of ballast under the three conditions tested in this study

4   can be significantly different, and will be presented in future publications.

5

6   **EFFECT OF AXIAL STRAIN ON SPECIMEN GEOMETRY CHANGE**

7   The measurement of volumetric strain, and tracking the corresponding

8   changes in specimen geometry during shear strength testing of large aggregate

9   particles, such as railroad ballast, can be very challenging. As already mentioned,

10 on-specimen deformation measurements using LVDTs was not carried out during the

11 current study to prevent damage to the instrumentation upon instant excessive bulging

12 of the specimen. However, information regarding volumetric strains and specimen

13 geometric changes during triaxial shear strength testing of ballast can be easily

14 extracted from numerical simulations. Changes in the radius of each membrane layer

15 as well as specimen volume with imposed axial strain for all the test configurations

16 are presented in Fig. 9. Corresponding information for new ballast was provided

17 elsewhere (Mishra et al. 2014). Fig.9 clearly shows that the initial radius of each

18 membrane layer was identical (152.4 mm or 6 in.), but underwent different change

19 patterns with gradual increases in axial strain. Note that membrane layer M8 behaved

20 differently than other layers due to boundary effects (see Fig. 9). Changes in the

21 membrane layer radius can be interpreted as bulging of the specimen at the

22 corresponding locations. Membrane layers M4 through M7 exhibited the largest

increase in radius for both reinforced as well as unreinforced cases. However, the

largest radius was 175.6 mm (M6) for the unreinforced case; 171.6 mm (M5) for the

triangular aperture geogrid reinforced case; and 167.0 mm (M6) for the square

aperture geogrid reinforced case. From Fig. 9, the radius increases for

geogrid-reinforced cases were more "uniform" compared to the unreinforced case.

This is a direct manifestation of the "restraining" effect of geogrids against lateral

movement. Note that for unreinforced specimens, particles near the specimen

mid-depth underwent large lateral movements, with particles near top and bottom of

specimen exhibiting no significant lateral movement. Fig. 9 also shows that gradual

increase in the axial strain initially resulted in a small reduction in the specimen

volume, followed by continued increase. The unreinforced specimen demonstrated the

highest degree of dilation, whereas the dilation for the specimen with a

square-aperture geogrid was the lowest. This is also indicative of the effectiveness of

geogrids as far as restrained lateral particle movement during shear strength testing is

concerned.

For better visualization of changes in specimen geometry with increasing axial

strain levels, Fig. 10 shows the front view of a DEM-generated triaxial ballast

specimen (degraded ballast without fines) reinforced with a triangular aperture

geogrid at three different axial strain levels. As shown in the figure, the maximum

bulging takes place slightly below the specimen mid-depth (location of geogrid

placement), which corresponds to layers M5 and M6. This visual representation is in

agreement with the trends in radius change reported in Fig. 9. Specimen configurations in DEM simulation and laboratory test under 10% strain are compared in Fig. 11.

Note that the particle reorientations at the ballast-geogrid interface can also have significant effects on the changes in specimen geometry with increasing axial strain levels. As an example, this can be illustrated considering two individual ballast particles from one of the DEM simulations. Fig. 12 shows two ballast particles (Particle A and Particle B) and their contacts with the geogrid element from the DEM simulation. Although both the particles remained in contact with the geogrid element throughout the triaxial shear strength test simulation, the type of particle rotation and reorientation at the ballast-geogrid interface with increasing axial strain was different for the two. Particle A exhibited a potential trend to climb over the geogrid element, particularly at relatively large (~ 6%) axial strain levels. However, Particle B on the other hand, tended to come into the geogrid aperture throughout the shearing procedure. Such detailed information regarding contact behavior obtained from the DEM simulations can be potentially used to optimize the combination of particle shape, geogrid rib shape, particle size, and aperture size, etc., thus maximizing effective interlocking between geogrids and aggregate particles.

SUMMARY AND CONCLUSIONS

This paper presented results of shear strength tests conducted on

geogrid-reinforced railroad ballast specimens using a large-scale triaxial test device.

Geogrids with triangular and square shape apertures were used to reinforce both new

and degraded (with and without fine particles smaller than 9.5 mm) ballast specimens.

Numerical simulations were performed using an aggregate image analysis-based

Discrete Element Method (DEM) modeling approach to demonstrate its capabilities

for studying geogrid-aggregate interlock reinforcement mechanisms.   The following

conclusions can be drawn from this study:

Both triangular and square-aperture geogrids were found to effectively

increase the peak deviator stress values for triaxial specimens prepared using the new

and degraded ballast materials. Highest shear strength values in the current study were

obtained for ballast specimens reinforced using the square-aperture geogrid. However,

it should be noted that the objective of this study was not to compare the

performances of different geogrid types, but rather to demonstrate the capabilities of

the DEM approach in simulating ballast reinforcement phenomenon. Accordingly,

further research is required to fully investigate aperture shape effects on the overall

geogrid reinforcement mechanism.

Specimens prepared using degraded ballast materials did not necessarily

exhibit lower shear strength values compared to those prepared using the new ballast

material under dry conditions. On the contrary, in most cases, specimens prepared

using the degraded ballast materials exhibited higher shear strength values under dry

conditions and similar loading and reinforcement conditions compared to those

prepared using the new ballast material. Specimens prepared with the degraded ballast

material without fines yielded the highest shear strength values under both

unreinforced as well as geogrid-reinforced configurations.

The aggregate imaging-based DEM simulation platform developed at the

University of Illinois could adequately simulate the stress-strain behavior of both

unreinforced and geogrid-reinforced ballast specimens under monotonic triaxial shear

strength tests. Some important information such as volumetric change and geometry

change due to specimen bulging, that are difficult to measure in the laboratory during

triaxial shear strength tests, can be easily extracted from DEM simulations. The DEM

approach also proved to be adequate in capturing contact behavior details at the

geogrid-aggregate interfaces. This aggregate imaging based DEM simulation platform

currently being further developed at the University of Illinois has the potential to

quantify individual effects of various geogrid properties, such as aperture shape and

size and rib dimensions, on the aggregate assembly.

ACKNOWLEDGMENTS

REFERENCES

Bathurst, R. J. and Raymond, G. P., 1987. *Geogrid Reinforcement of Ballasted Track*. Transportation Research Record. No. 1153: 8-14.

Brown, S. F., Kwan, J. and Thom, N. H., 2007. *Identifying the Key Parameters that Influence Geogrid Reinforcement of Railway Ballast*. Geotextiles and Geomembranes, 25(6):326-335.

Chen, C., McDowell, G.R., and Thom, N.H., 2012. *Discrete Element Modeling of cyclic loads of geogrid-reinforced ballast under confined and unconfined condition*. Geotextiles and Geomembranes, 35(12):76-86.

Ghaboussi, J. and Barbosa, R. 1990. *Three dimensional discrete element method for granular materials*. International J. for Numerical and Analytical Methods in Geomechanics, 14: 451-472.

Indraratna, B., Khabbaz, H., Salim, W. and Christie, D., 2006. *Geotechnical Properties of Ballast and the Role of Geosynthetics in Rail Track Stabilization*.

Journal of Ground Improvement, 10(3): 91-102.

Indraratna, B., Thakur, P.K., and Vinod, J.S., 2010. *Experimental and Numerical Study of Railway Ballast Behavior under Cyclic Loading*. International Journal of Geomechanics, ASCE, 10(4):136-144.

Lee, S. J., Hashash, Y.M.A., and Nezami, E.G., 2012. *Simulation of Triaxial Compression Test with Polyhedral Discrete Elements*. Computers and Geotechnics, 43:92-100.

Lu, M. and McDowell, G.R., 2010. *Discrete Element Modelling of Railway Ballast under Monotonic and Cyclic Triaxial Loading*. Geotechnique, 60(6):459-467.

McDowell, G.R., Harireche, O., Konietzky, H., Brown, S.F., and Thom, N.H., 2006. *Discrete Element Modelling of Geogrid-Reinforced Aggregates*. In Proceedings of the Institution of Civil Engineers—Geotechnical Engineering, 159: 35-48.

Mishra, D., Kazmee, H., Tutumluer, E., Pforr, J., Read, D., and Gehringer, E., 2013. *Characterization of Railroad Ballast Behavior Under Repeated Loading: results from New Large Triaxial Test Setup*. Transportation Research Record: Journal of the Transportation Research Board, Transportation Research Board of the National Academies, Washington, D.C., Vol. 2374, pp. 169-179.

Mishra, D., Qian, Y., Kazmee, H., Tutumluer, E., 2014. *Investigation of Geogrid-Reinforced Railroad Ballast Behavior Using Large-Scale Triaxial Testing and Discrete Element Modeling*. Transportation Research Record: Journal of the Transportation Research Board, Transportation Research Board of the National Academies, Washington, D.C. (accepted)

Nezami, E. G., Hashash, Y.M.A., Zhao, D. and Ghaboussi, J., 2007. *Simulation of front end loader bucket-soil interaction using discrete element method*. International Journal for Numerical and Analytical Methods in Geomechanics, 31(9): 1147 – 1162.

Pan, T., Tutumluer, E., and Carpenter, S.H. 2006. *Effect of Coarse Aggregate Morphology on Permanent Deformation Behavior of Hot Mix Asphalt*. Journal of Transportation Engineering, 132(7): 580-589.

Qian, Y., Tutumluer, E., and Huang, H., 2011. *A Validated Discrete Element Modeling Approach for Studying Geogrid-Aggregate Reinforcement Mechanisms*. Geo-Frontiers 2011, ASCE Geo-Institute. March 13-16, Dallas, TX.

Qian, Y., Mishra, D., Tutumluer, E., Kwon, J., 2013a. *Comparative Evaluation of Different Aperture Geogrids for Ballast Reinforcement through Triaxial Testing and Discrete Element Modeling*. Geosynthetics 2013. April 1-4, Long Beach, CA.

Qian, Y., Mishra, D., Tutumluer, E., Kwon, J., 2013b. *Discrete Element Modeling of Ballast Reinforced with Triangular Aperture Geogrid*. 9th International Conference on Bearing Capacity of Roads, Railways and Airfields. June 25-27, Trondheim, Norway.

Qian, Y., Lee, S.J., Tutumluer, E., Hashash, Y. M.A., Mishra, D., and Ghaboussi, J., 2013c. *Discrete Element Method for Simulating Ballast Shear Strength from Large Scale Triaxial Tests*. Journal of the Transportation Research Board, Transportation Research Board of the National Academies, Washington, D.C., No. 2374: 126-135.

Qian, Y., Boler, H., Moaveni, M., Tutumluer, E., Hashash, Y. M.A., and Ghaboussi, J.,

2014. *Characterizing Ballast Degradation through Los Angeles Abrasion Test and Image Analysis*. Transportation Research Record: Journal of the Transportation Research Board, Transportation Research Board of the National Academies, Washington, D.C., No. 2448: 142-151.

Rao, C., Tutumluer, E. and Kim, I.T., 2002. *Quantification of Coarse Aggregate Angularity Based on Image Analysis*. Transportation Research Record. No. 1787: 193-201.

Raymond, G. and Ismail, I., 2003. *The Effect of Geogrid Reinforcement on Unbound Aggregates*. Geotextiles and Geomembranes, 21(6): 355-380.

Selig, E.T. and Waters, J.M., 1994. *Track Geotechnology and Substructure Management*. Thomas Telford, Ltd.

Tutumluer, E., Huang, H., Hashash, Y.M.A., and Ghaboussi, J., 2006. *Aggregate Shape Effects on Ballast Tamping and Railroad Track Lateral Stability*. In Proceedings of the AREMA Annual Conference, Louisville, Kentucky, USA, September 17-20.

Tutumluer, E, Huang, H., and Bian, X. 2009. *Research on the Behavior of Geogrids in Stabilization Applications,* Proc., Jubilee Symposium on Polymer Geogrid Reinforcement, September 8, 2009, London, UK.

Tutumluer, E., Qian, Y., Hashash, Y. M.A., Ghaboussi, J., and Davis, D., 2013. *Discrete Element Modeling of Ballasted Track Deformation Behavior*. International Journal of Rail Transportation, 1(1-2): 57-73.

Zhao, D., Nezami, E.G., Hashash, Y.M.A., and Ghaboussi, J., 2006.

1 *Three-dimensional discrete element simulation for granular materials*. Engineering

2 Computations, 23(7): 749-70.

3

4

5

6

7

8

9

10

11

12

13

14

15

16

17

18

19

20

21

22

1

2

3

4   **TABLE 1. Triaxial Test Specimen Details and Shape Properties of Large–sized**

5   **(above 9.5-mm or 3/8-in.) Particles**

6

	New ballast	**Degraded ballast without fines**	**Degraded ballast with fines**
Average Angularity Index (AI in degrees)	440	278	278
Average Flat & Elongated (F&E) Ratio	2.3	1.9	1.9
Average Surface Texture (ST) Index	1	1.3	1.3
Coefficient of Uniformity (C_u)	1.46	1.79	350
Coefficient of Curvature (C_c)	0.97	1.13	4.02
Specimen height	610 mm	610 mm	610 mm
Specimen diameter	305 mm	305 mm	305 mm
Specimen weight	70 kg	73 kg	94 kg
Compaction time	16 seconds	16 seconds	16 seconds
Void ratio (e)	0.68	0.61	0.25

7

8

9

10

11

12

13

14

1

2

3

4 **TABLE 2. Properties of Geogrids Used**

5

	Square Aperture	Triangular Aperture	
	Side	Longitudinal	Diagonal
Aperture Dimensions (mm)	65	60	60
Ultimate QC Strength (kN/m)	30		
Junction Efficiency (percentage)		93	
Radial Stiffness (kN/m@0.5% strain)		350	

6

7

8

9

10

11

12

13

14

15

16

17

18

19

1

2

3

4 **TABLE 3. Model parameters used in ballast DEM triaxial test simulations**

5

DEM Model Parameter	Value
Inter-particle Friction Angle	31°
Normal Contact Stiffness	20 MN/m
Shear Contact Stiffness	10 MN/m
Global Damping	0.06
Contact Damping	0.03
Time Step	2.70×10^{-6} sec

6

7

8

9

10

11

12

13

14

15

16

17

18

19

1

2

3

4

5

6

7 **TABLE 4. Peak Strength Values from Laboratory Tests and DEM Simulation**
8   **Predictions**
9

	Ballast Type	Unreinforced (kPa)	Triangular Aperture Geogrid Reinforced (kPa)	Square Aperture Geogrid Reinforced (kPa)
Lab	Clean	590	643	705
	Degraded w/o fines	709	786	894
	Degraded w/fines	570	664	836
DEM	Clean	604	709	912
	Degraded w/o fines	693	813	880

10

11

12

13

14

15

16

17

18

19

1

2

3

4

5

6

Beginning of
Ballast Service Life

Ballast Degradation

End of
Ballast Service Life

New Ballast FI=0

Fouled Ballast 0<FI<40

Fouled Ballast FI=40

7
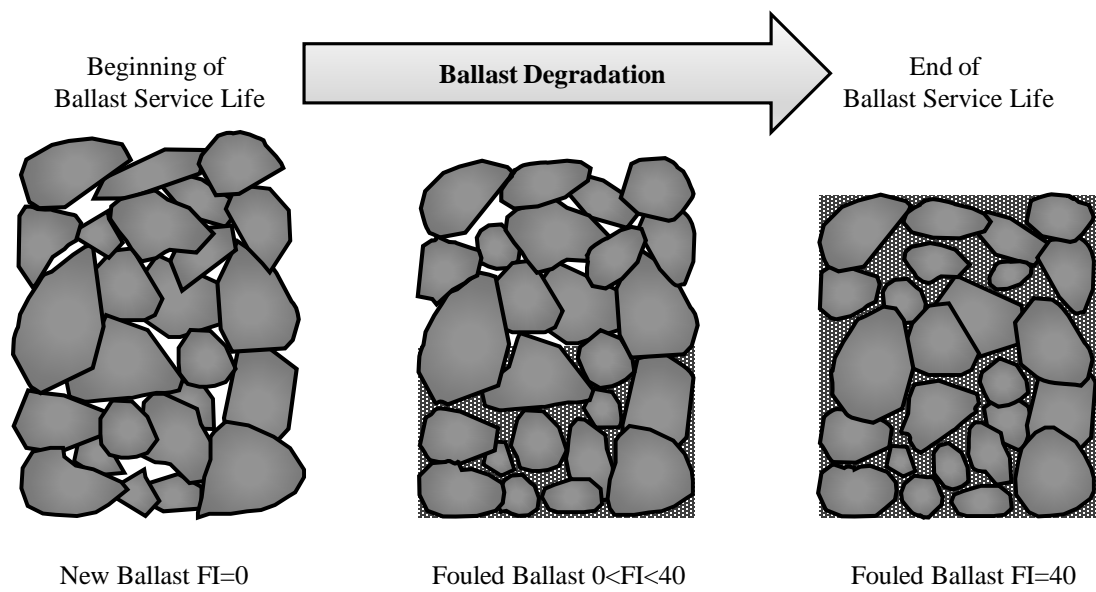
8   **FIG. 1.   Schematic drawing of ballast degradation**

9

10

11

12

13

14

15

16

1

2

3

4

5

6

7

8   **FIG. 2.   Triaxial shear strength test setup**

9

10

1

2

3

4

5

6

7

8

9

10

11
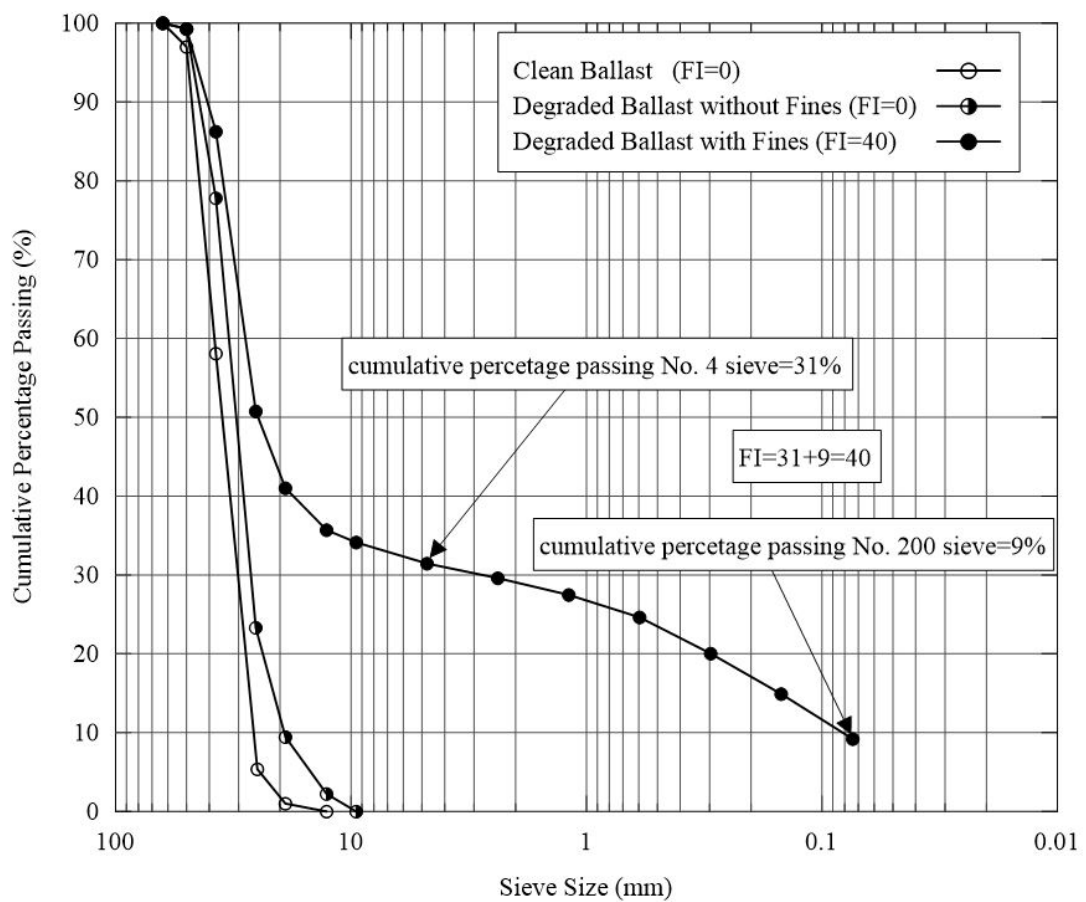
FIG. 3. Particle size distributions of clean and degraded ballast aggregates

1

2

3

4

5

6

7

8

9

10

11
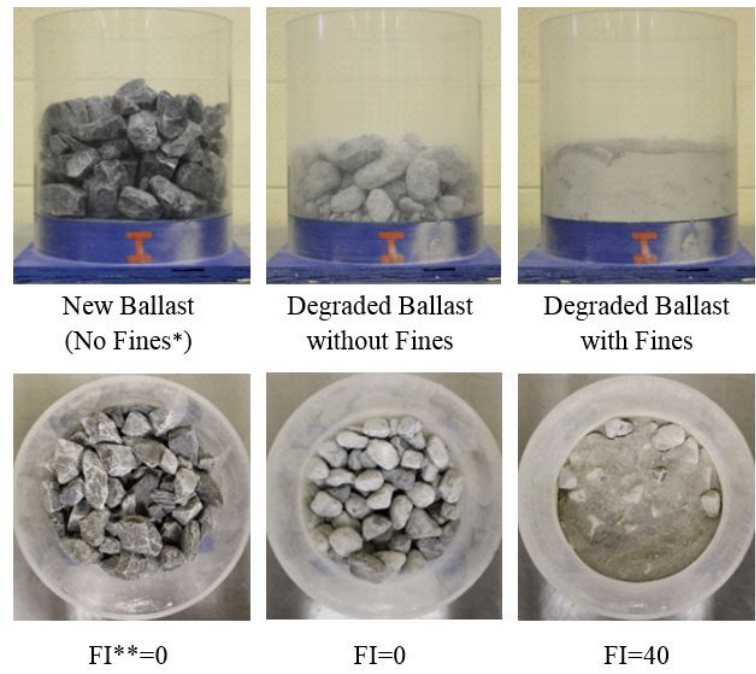
FIG. 4. Photos of side and top views of new and degraded aggregate packing

14

1

2

3

4

5

6

7

8

Ballast Particle   **Enhanced UIAIA**   **3D Polyhedron used in DEM**

9

10
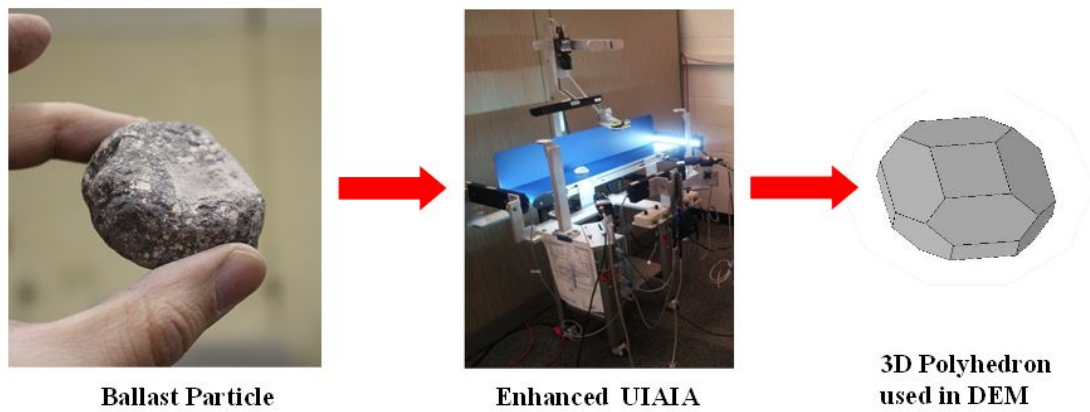
11 **FIG. 5. Conceptual approach for aggregate imaging-based railroad ballast**
12 **particle generation for discrete element method (DEM) simulations**

13

14

15

16

17

18

1

2

3

4

5

6

7

8

9

10
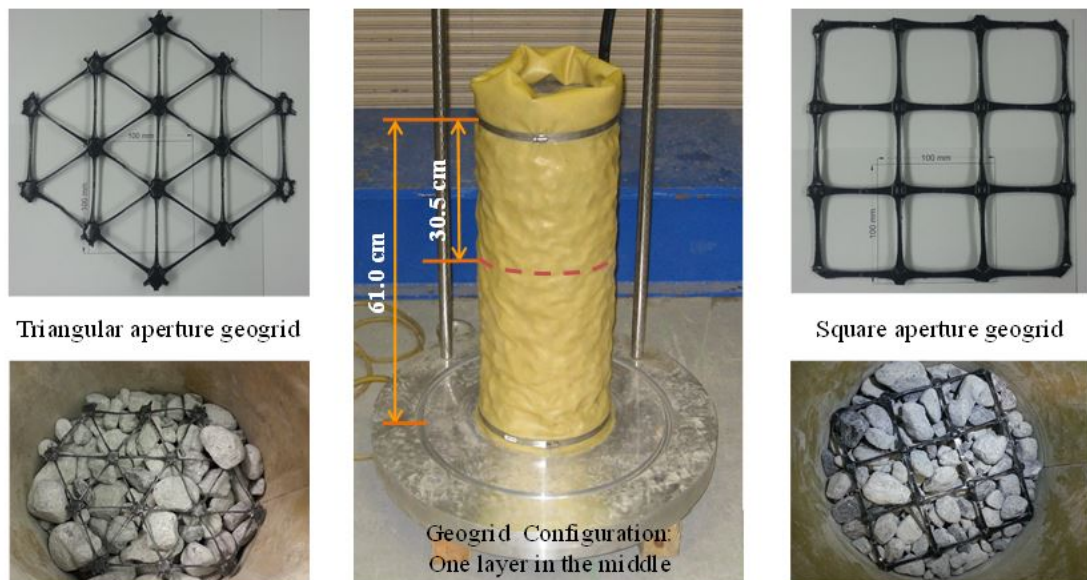
11 **FIG. 6. Triangular and square aperture geogrids used in creating triaxial test**
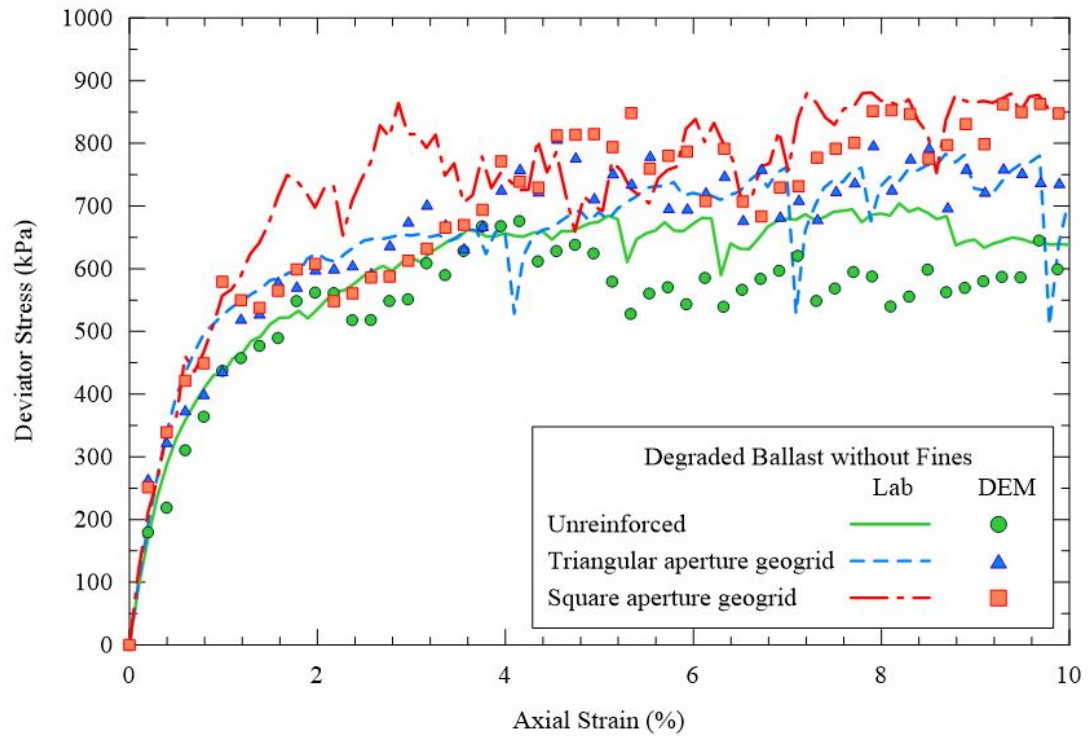12   **specimens**

13

14

15

16

17

1

2

3

4

5

6

7

Triangular aperture geogrid

Membrane elements

305 mm

610 mm

305 mm

Ballast particles

M1
M2
M3
M4
M5
M6
M7
M8

Square aperture geogrid
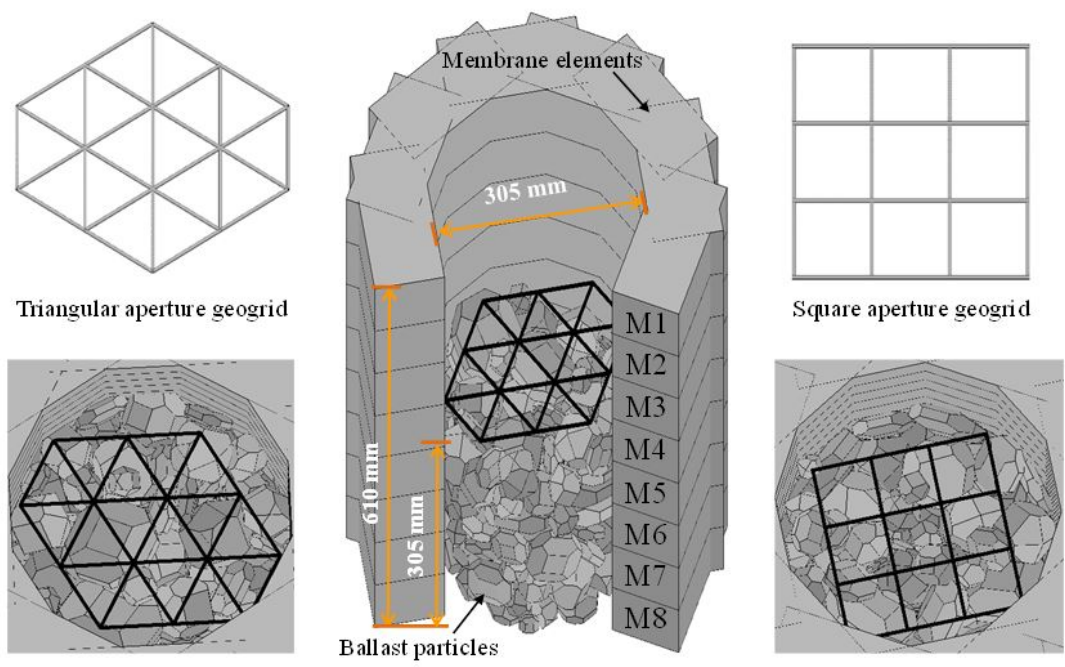
8
9
10 **FIG. 7. Geogrids and triaxial ballast specimen established in DEM simulations**

11

12

13

14

15
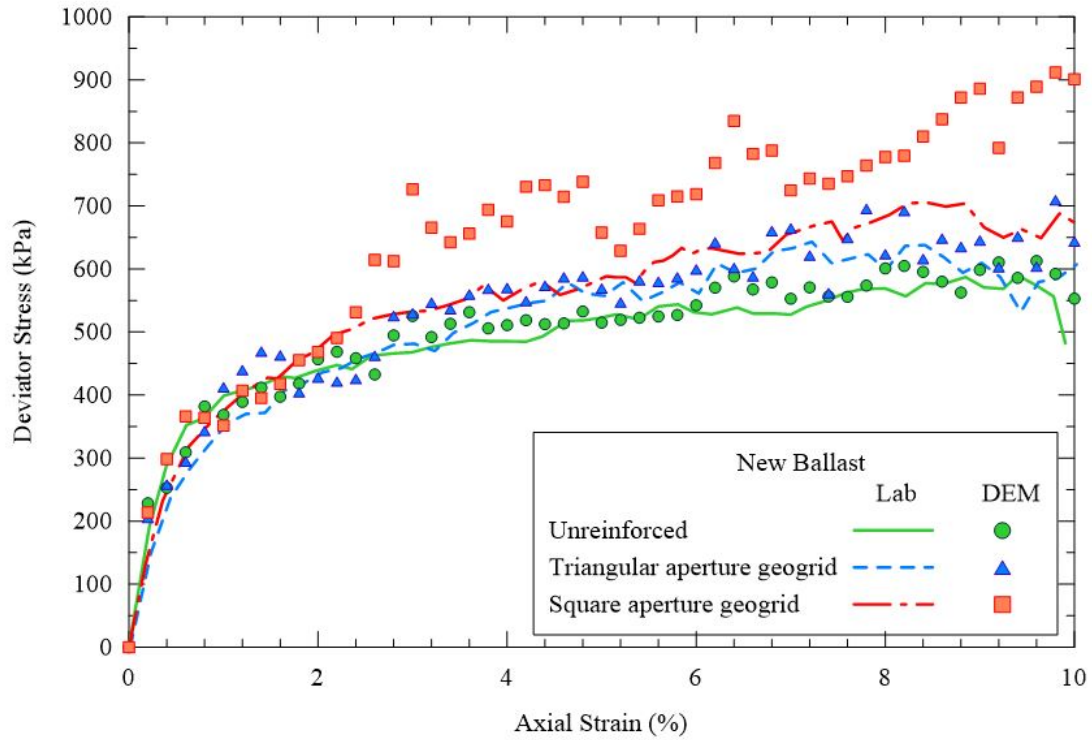
1
2
3   (a) Strength tests and DEM simulations results of new ballast
4

5
6
7   (b) Strength tests and DEM simulations results of degraded ballast without fines
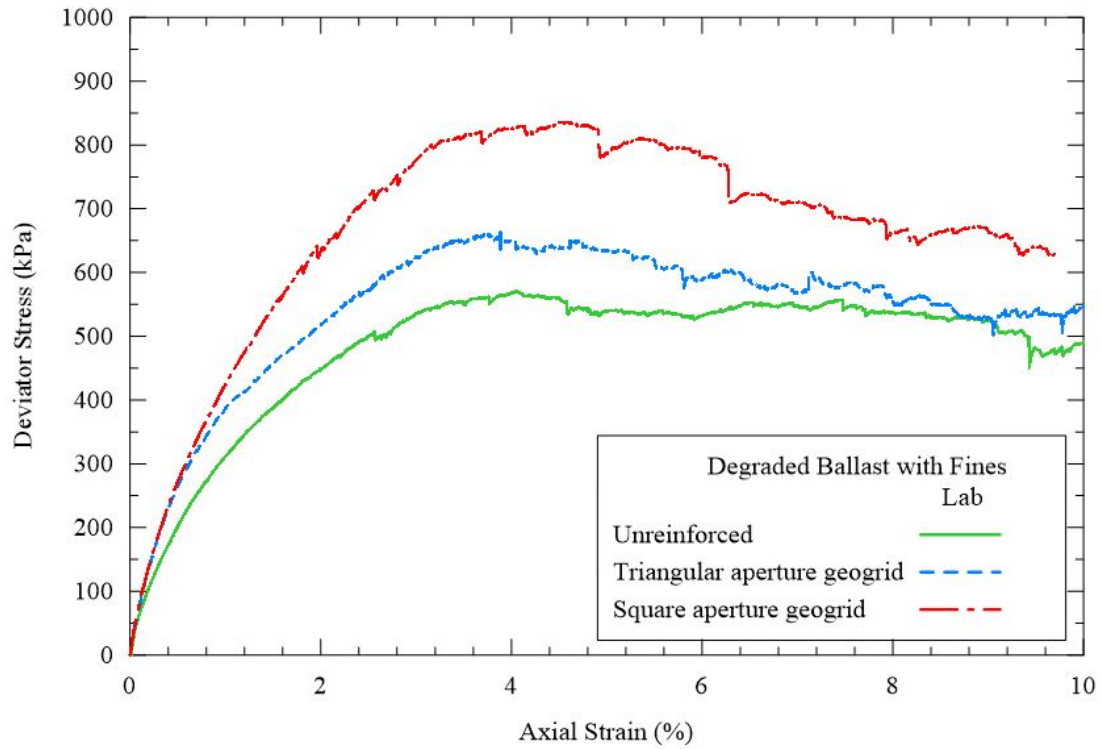
(c) Strength tests and DEM simulations results of degraded ballast with fines

FIG. 8. Laboratory triaxial ballast strength tests and DEM simulation results (Note that only laboratory data presented for the Degraded Ballast Material with Fines)
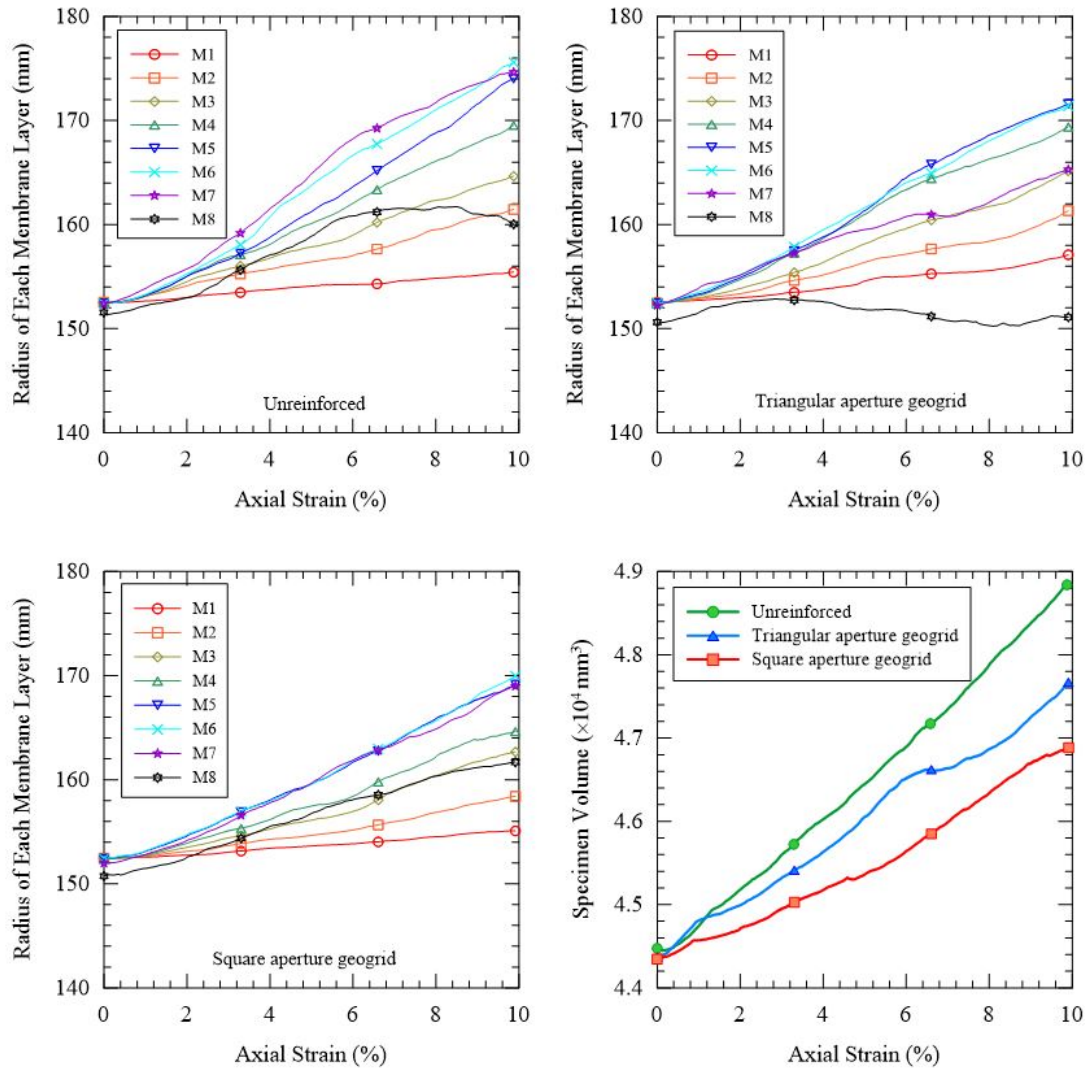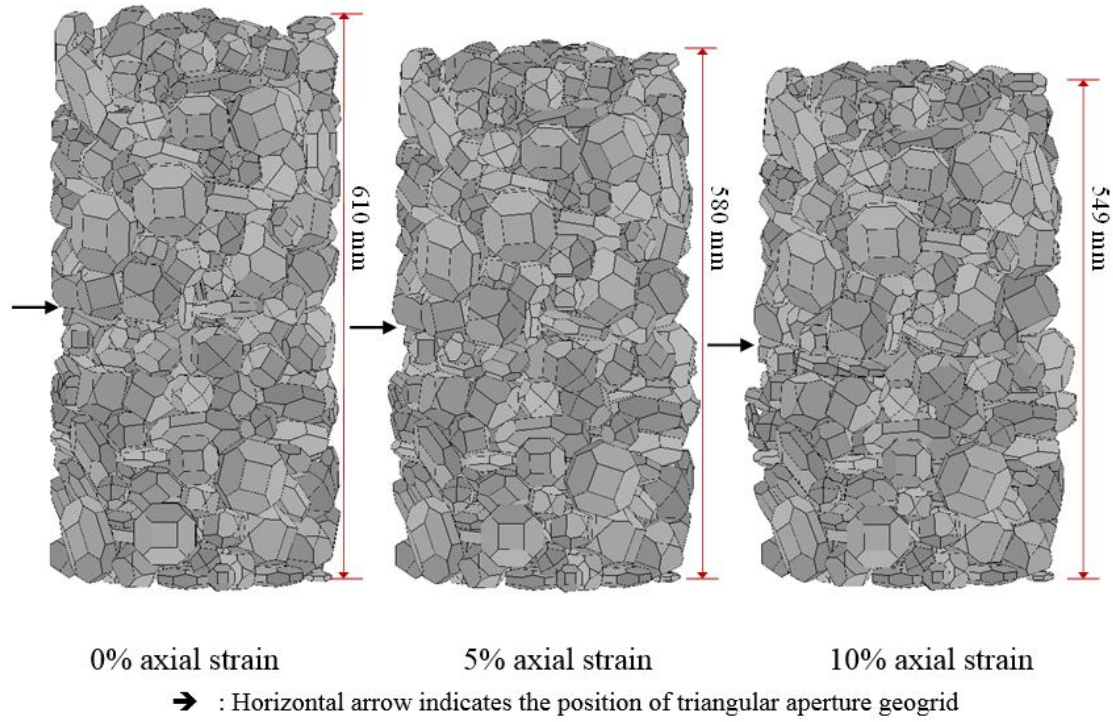
1

2
3   **FIG. 9. Volume and radius of each membrane layer element in test specimens**
4   **with degraded ballast without fines computed in DEM simulations**
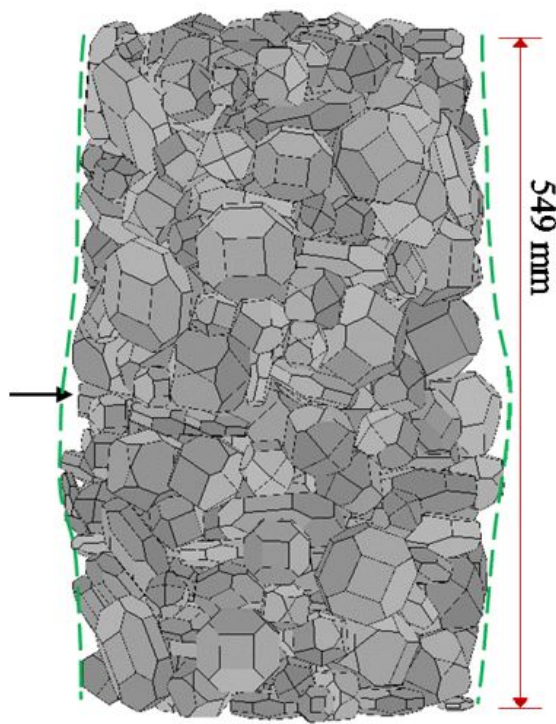
5

6

7

8

9

10

11

1

2

3

0% axial strain   5% axial strain   10% axial strain

➔ : Horizontal arrow indicates the position of triangular aperture geogrid

FIG. 10. Front view of DEM simulation of the triangular aperture geogrid reinforced specimen of the degraded ballast without fines

4

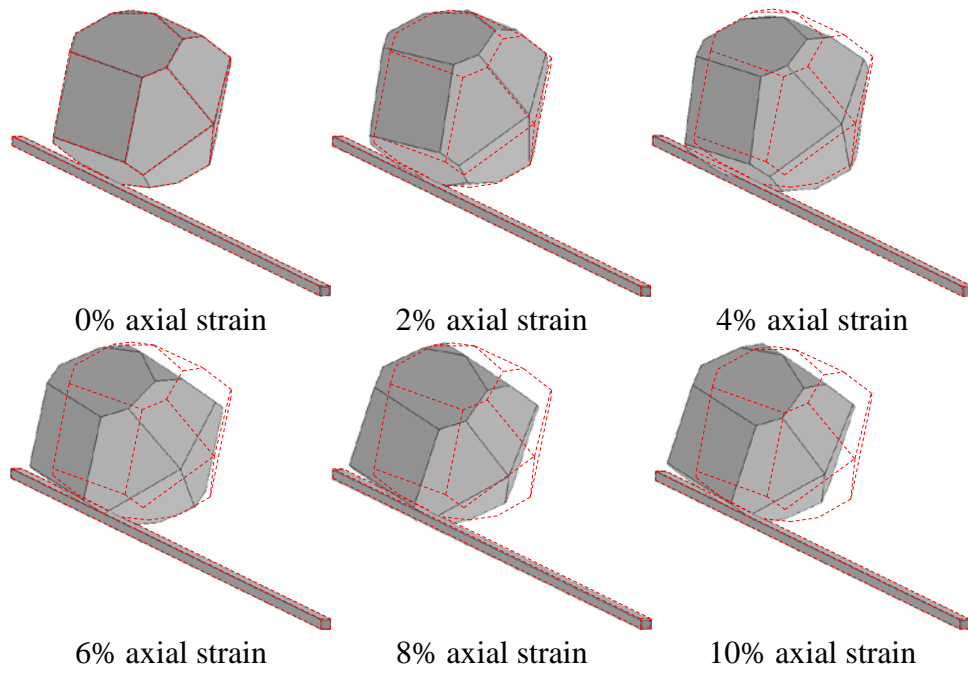5

6

7

8

9

10

11

12

13
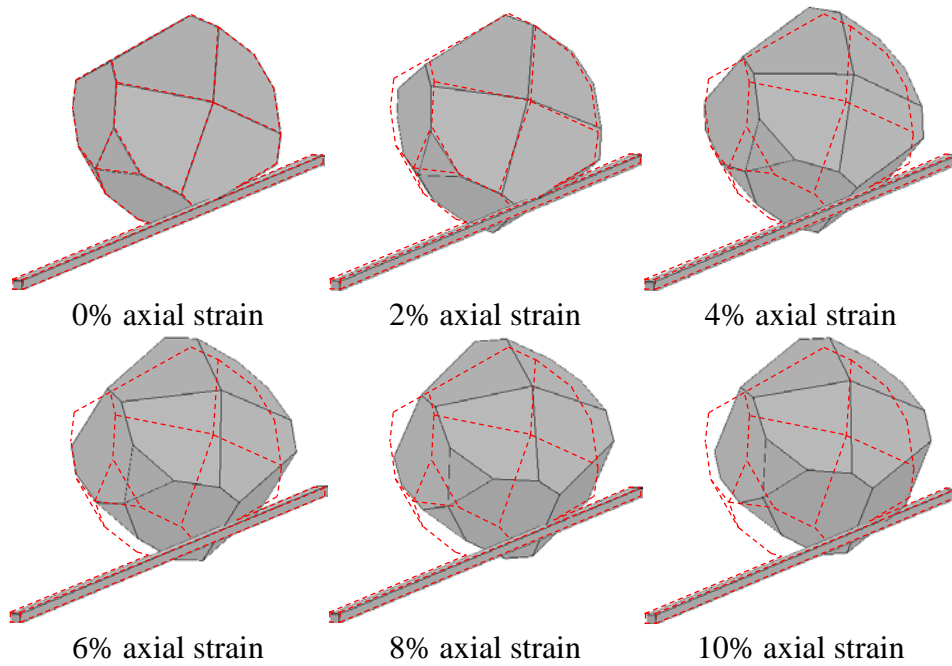
14

15

(a) Specimen in DEM   (b) Specimen in Lab

FIG. 11. Deformed ballast specimen configuration of the triangular aperture geogrid reinforced specimen of the degraded ballast without fines: (a) Laboratory test; (b) DEM simulation

0% axial strain 2% axial strain 4% axial strain

6% axial strain 8% axial strain 10% axial strain

1   (a) Particle A and its contacts with geogrid element
2   (red dash line indicates original position)
3

0% axial strain 2% axial strain 4% axial strain

6% axial strain 8% axial strain 10% axial strain

4   (b) Particle B and its contact with geogrid element
5   (red dash line indicates original position)
6
7 **FIG. 12. Two single particles analyzed and their contacts with geogrid element in**
8   **DEM simulations of a shear strength test**